NASA TECHNICAL NOTE

NASA TN D-7324

NASA TN D-7324

OXIDATION AT THROUGH-HOLE DEFECTS IN FUSED SLURRY SILICIDE COATED COLUMBIAN ALLOYS FS-85 AND Cb-752

by Stanley R. Levine

Lewis Research Center and
U.S. Army Air Mobility R&D Laboratory
Cleveland, Ohio 44135

NATIONAL AERONAUTICS AND SPACE ADMINISTRATION • WASHINGTON, D. C. • JULY 1973

1. Report No.	2. Government Accession No.	3. Recipient's Catalog No.
NASA TN D-7324		

4. Title and Subtitle	5. Report Date
OXIDATION AT THROUGH-HOLE DEFECTS IN FUSED SLURRY SILICIDE COATED COLUMBIUM ALLOYS FS-85 AND Cb-752	July 1973
	6. Performing Organization Code

7. Author(s)	8. Performing Organization Report No.
Stanley R. Levine	E-7330
	10. Work Unit No. 501-21

9. Performing Organization Name and Address	11. Contract or Grant No.
NASA Lewis Research Center and U. S. Army Air Mobility R&D Laboratory Cleveland, Ohio 44135	

12. Sponsoring Agency Name and Address	13. Type of Report and Period Covered *
National Aeronautics and Space Administration Washington, D. C. 20546	Technical Note
	14. Sponsoring Agency Code

15. Supplementary Notes

16. Abstract

Metal recession and interstitial contamination at 0.08-centimeter-diameter through-hole intentional defects in fused slurry silicide coated FS-85 and Cb-752 columbium alloys were studied to determine the tolerance of these materials to coating defects. Five external pressure re-entry simulation exposures to 1320° C and 4.7×10^3 N/m^2 (maximum pressure) resulted in a consumed metal zone having about twice the initial defect diameter for both alloys with an interstitial contamination zone extending about three to four initial defect diameters. Self-healing occurred in the 1.33×10^1 N/m^2, 1320° C exposures and to a lesser extent in internal pressure re-enetry cycles to 1320° C and 1.33×10^2 N/m^2 (maximum pressure).

17. Key Words (Suggested by Author(s))

Columbium alloys
Coatings
Silicides
Oxidation
Thermal protection

18. Distribution Statement

Unclassified - unlimited

19. Security Classif. (of this report)	20. Security Classif. (of this page)	21. No. of Pages	22. Price*
Unclassified	Unclassified	34	$3.00

* For sale by the National Technical Information Service, Springfield, Virginia 22151

OXIDATION AT THROUGH-HOLE DEFECTS IN FUSED SLURRY SILICIDE COATED COLUMBIUM ALLOYS FS-85 AND Cb-752

by Stanley R. Levine

Lewis Research Center and
U. S. Army Air Mobility R&D Laboratory

SUMMARY

The rates of intentional defect growth and interstitial contamination at a nominal 0.08-centimeter through-hole in fused slurry silicide coated columbium alloys FS-85 and Cb-752 were studied. Specimens were exposed in a tube furnace to either (1) 1 or 5 hours of exposure at 1125° or 1320° C and at 1.33×10^{1} or 1.33×10^{3} newtons per square meter (0.1 or 10 torr) or (2) one or five cycles of reentry simulation exposure to a maximum temperature of 1320° C under external or internal pressure reentry vehicle conditions.

The metal recession and interstitial contamination processes were followed by metallographic and microhardness measurements. Weight change behavior, an X-ray diffraction analysis of surface oxides, spectrographic and XRD analyses of condensed oxides, and an electron microprobe analysis of the defected region were performed to clarify the observed self-healing process. The amount of metal recession was about 15 percent greater for coated FS-85 than for coated Cb-752 in isothermal exposures at 1320° C and 1.33×10^{3} newtons per square meter. In external pressure reentry simulation exposures the metal recession was about the same for both alloys. The extent of interstitial contamination was about 15 percent greater for FS-85 than for Cb-752. The interstitial contamination zone extended about three to four initial defect diameters after five reentry cycles. Self-healing occurred in the 1.33×10^{1} newtons per square meter, 1320° C exposures and to a lesser extent in the internal pressure reentry cycles.

INTRODUCTION

Reradiative heat shields offer a multimission thermal protection system (TPS) capa-

bility for atmospheric reentry vehicles. For vehicle areas above 1100° C, fused slurry silicide coated columbium alloys have been investigated as a candidate material (ref. 1). Since reentry vehicles are exposed to high velocity particle impacts during space flight (ref. 2), reentry, and landing, the brittle silicide coating may be damaged. In addition, the closed passages of corrugation stiffened panels are not amenable to thorough inspection, and small thin or damaged areas of the coating may go undetected. Damaged or thin areas of the coating may eventually expose the substrate to oxidation and interstitial oxygen contamination during subsequent reentry exposures. However, recent mechanical property tests have shown that specimens with small intentional coating defects can resist a number of simulated reentry exposures before ductility and/or strength are seriously affected. One of the reasons that FS-85 was selected as a best TPS columbium alloy for evaluation was that it suffers less degradation of mechanical properties than C-129Y or Cb-752 at such intentional defects (ref. 3). The critical factor for face-sheet damage on heat shield panels is plasma ingestion at the defect. Thus, the rate of burnthrough at a defect and the rate of growth of the hole are the most important parameters. In addition, the ability of the coating to self-heal and the conditions under which this is possible are important considerations when using coated columbium alloys. At the present time, neither the rates of defect growth and interstitial contamination nor the self-healing ability of the fused slurry silicide coatings currently under consideration are well characterized.

The primary purpose of this study was to investigate the kinetics of interstitial contamination and defect growth at a defect (nominal 0.08-cm-diameter through-hole) in commercially applied, fused slurry silicide coated columbium alloys during simulated reentry as achieved by furnace exposures in air. The defect size was relatively large-about twice the thickness of the substrates. A second purpose of this study was to determine if self-healing could occur at the defect site and, if so, the nature of the self-healing mechanism.

Commercially applied iron-chromium-silicon (HiTempCo, Inc. R512E) and iron-chromium-hafnium-silicon (Vac-Hyd Corp. VH-109) coatings on 0.033-centimeter-thick columbium alloy Cb-752 and R512E on 0.028- and 0.033-centimeter-thick alloy FS-85 coupons were defected by grit blasting a nominal 0.08-centimeter hole through the center of the coupon. The defected specimens were exposed to either (1) one or five reentry vehicle internal or external pressure reentry simulation profiles to a maximum temperature of 1320° C or (2) 1 or 5 hours of isothermal, isobaric exposure at 1125° or 1320° C and at 1.33×10^{1} or 1.33×10^{3} newtons per square meter (N/m^2) (0.1 or 10 torr). The 1320° C value was chosen because it is near the peak TPS use-temperature for coated columbium alloys while 1125° C is close to the middle of the reactive temperature range of silicide coatings. The amount of defect growth was determined by metallographic measurements and microhardness traverses of the substrate. The rate of inter-

stitial contamination was compared with predicted values determined from a simplified model. In addition, electron microprobe (EMP) line scans on selected specimens and an analysis of coating surface oxides by X-ray diffraction (XRD) were performed to clarify the self-healing mechanism. Spectrographic and XRD analyses of vaporized oxides were also performed.

EXPERIMENTAL PROCEDURES

Materials

The columbium alloys used in this study were FS-85 (nominally Cb-28Ta-10W-1Zr) and Cb-752 (nominally Cb-10W-2.5Zr). Both alloys were received as 100-percent recrystallized sheet. Ingot and sheet analyses are listed in table I.

The alloys were sheared into 3.8 by 1.9 centimeter coupons and finished on the edges by the coating vendors. R512E (Si-20Cr-20Fe) was applied by HiTempCo, Inc. The duplex VH-109 coating (Si-Hf-Ta followed by Si-Hf-Cr-Fe) was applied by Vac-Hyd Processing Corporation. Data on the alloys and their respective coatings are presented in table II.

Testing Procedure

Defects were introduced in the coated specimens by grit blasting with 50-micrometer alumina particles through a 0.071-centimeter-diameter hole in a soft copper mask until a hole through the specimen was visible. The grit blasted holes were generally elliptical with sloped sides. The holes were then reamed with a 0.071-centimeter-diameter drill. The resulting holes were nominally 0.08 centimeter and varied from a circular shape having the drill dimensions to a slightly larger elliptical shape. To determine the hole size the diameter or major and minor ellipse axes were measured with an optical comparator.

The defected specimens were placed on a fused slurry silicide coated columbium support rod and inserted into the mullite muffle of a graphite heating element tube furnace. Four coupons were exposed in each run - one of each coating substrate combination. The exposures were either (1) one isothermal, isobaric exposure cycle of 1 or 5 hours in duration or (2) one or five reentry simulation exposure cycles to a peak temperature of 1320^{o} C and a pressure profile approximating either the internal or external conditions on a reentry heat shield as shown in figure 1. The following isothermal, iso-

baric cycles were used: 1125° C at 1.33×10^{1} or 1.33×10^{3} N/m^2 (0.1 or 10 torr), and 1320° C at 1.33×10^{1} or 1.33×10^{3} N/m^2 total pressure.

Analyses

After exposure the specimens were examined and weighed to the nearest 0.1 milligram. The 1320° C, 1.33×10^{1} N/m^2 exposures resulted in volatilization of considerable quantities of oxide. The condensed oxide was analyzed by emission spectrography and XRD. XRD analyses of surface oxides on selected samples were also performed.

The specimens were sectioned transverse to the original sheet rolling direction and mounted in epoxy. The metallographic mounts were ground on progressively finer silicon carbide papers until the center of the defect was reached. The specimens were then final polished and swab etched with a solution of equal volumes of hydrofluoric acid, nitric acid, and glycerol.

Microhardness traverses along the substrate centerline were made in a radial direction from the center of the defect. A Tukon microhardness tester with a Knoop indenter and a 200-gram load was used (magnification, ×250). Filar micrometer measurements were made of the indentations, their location with respect to the metal-oxide interface, the thickness of the oxide layer in the defect, the diameter of the hole, and the slope of the sides of the hole. To establish the effect of exposure, the initial defect diameter d_0 was established by the approach shown in figure 2. The initial average minimum defect diameter d_i was measured optically before exposure. The initial defect diameter along the substrate centerline was computed by assuming the shape of the hole was not significantly changed by exposure and by using the equations in figure 2.

Photomicrographs of selected specimens were taken at ×100. Electron microprobe line scans of the substrate and oxide formed in the defect were made in a radial direction from the center of the defect on some specimens. The elements scanned were columbium, oxygen, silicon, chromium, and iron.

RESULTS AND DISCUSSION

Macroscopic Behavior

The typical weight change behavior of these systems is represented by the data for R512E on FS-85 presented in figure 3. Since the defect area was much smaller than the specimen surface area, any locally heavy oxidation at the defect made an insignificant contribution to the total weight change. The oxide scales formed under external pressure conditions were thicker than under internal pressures. The oxides were primarily

Cb_2O_5, complex columbates, and silica on R512E coatings, and HfO_2, columbates, chromia, and silica on VH-109 as shown in table III. Generally, no obvious growth of the defect occurred in five reentry cycles, and after external pressure exposures the defects tended to fill with substrate oxides. In the 1.33×10^1 N/m^2, 1320° C exposure, active oxidation occurred with rapid loss of silicon (as SiO) from the coating as shown by the analyses of collected oxide condensates. Gravimetric data indicated that active oxidation also occurs during the first few reentry exposures under internal pressure conditions.

Behavior at the Defects

Photomicrographs of a typical series of defected and exposed specimens are shown in figures 4(a) to (*l*). The photographs are of a plane through the center of the defect at ×100. The material is R512E coated 0.028-centimeter FS-85.

Microhardness traverses and filar micrometer measurements of metal recession and defect diameter were made along the substrate centerlines of all systems. The results of the metallographic measurements are listed in table IV. The list includes the calculated initial radius of the defect and the amount of radial metal recession at the defect for each alloy-coating-exposure condition.

Metal recession. - In the 1.33×10^3 N/m^2 and external pressure exposures where significant metal recession was observed, a columbium oxide (CbO_2) layer formed on the exposed substrate in either 1 hour or 1 cycle of exposure. Additional exposure resulted in negligible additional growth of this oxide layer.

Metal recession data for oxidation at the defects in 1.33×10^3 N/m^2 (10 torr) isothermal and internal pressure reentry simulation cycles are plotted in figure 5 for each alloy coating combination. From these figures it is apparent that any difference in metal recession rates between alloy thicknesses or between coatings is masked by scatter in the data. Linear regression analyses of combined data for each alloy were performed. The regression lines were forced through the origin. The average correlation coefficients were 0.90, 0.97, and 0.97 for linear, parabolic, and cubic equations, respectively. As will be shown later, additional evidence for parabolic behavior was obtained from the locations of silicon concentrations in the growing oxide. On this basis the parabolic equation was selected for the graphs in figure 5.

A comparison of figure 5(a) with 5(c) indicates that the amount of metal recession for FS-85 is about 15 percent higher than for Cb-752 in isothermal exposures at 1320° C; in the 1125° C exposures the reverse is true with the metal recession rate for Cb-752 about 50 percent greater than for FS-85. In reentry simulation exposures metal recessions for the two alloys were about the same.

Interstitial contamination and oxygen diffusion. - Interstitial contamination was determined from microhardness traverses along the substrate centerline in a radial direction from the center of the defect. A typical family of such traverses is shown in figures 6(a) to (f). In order to relate the microhardness traverses in figure 6 to interstitial oxygen content, a series of oxygen dopings of alloy FS-85 were made according to the procedure given by Barrett (ref. 4). Prior experience indicates that the difference between air and oxygen doping is insignificant. A plot of microhardness against oxygen content as determined by weight gain measurements is given by the upper line in figure 7. Two samples were checked by oxygen fusion analysis. Typical agreement between oxygen fusion and weight gain measurements was ±0.14 atom percent. The as-coated substrates were softer than the as-received sheet since the former were brought to equilibrium at the coating fusion temperature which is higher than the sheet recrystallization temperature. The doped specimens were annealed for 5 minutes in vacuum at the coating fusion temperature (1415° C) to produce equilibrium conditions similar to those in the as-coated sheet. The results, plotted as the lower line in figure 7, were used to relate microhardness to oxygen content. As can be seen from figure 6, a Knoop microhardness number of 300 corresponds approximately to the mean microhardness level observed in the interstitially contaminated defected specimens and represents a significant increase in oxygen content (fig. 7). The microhardness level $KHN_{200g} = 300$ was selected as an indicator of the extent of interstitial contamination. At this microhardness level the substrate ductile-brittle transition temperature is above room temperature (ref. 5).

The radial locations r with $KHN_{200g} = 300$ are listed in table IV as dimensionless positions r/r_0, where r_0 is the initial radius of the defect. As can be seen from the listed data, the effect of FS-85 thickness is not separable from scatter in the data. The effect of coating type on contamination in Cb-752 is also not separable from scatter. Data for the respective alloys were combined and fitted to equations by regression analysis. For convenience the normalized abscissa t/r_0^2 (time/initial radius^2) was used since the progress of the interstitial contamination is inversely proportional to a function of the square of the initial radius of the defect. The equations examined for regression analysis of the data were

$$\frac{r}{r_0} = m_1\left(\frac{t}{r_0^2}\right)^{1/n} + b_1 \qquad (1)$$

where $n = 1$ to 5 and

$$\frac{r - r_0}{r_0} = m_2\left(\frac{t}{r_0^2}\right)^{1/b_2} \tag{2}$$

When equation (1) was used the average correlation coefficient reached a maximum of 0.941 when n was 3 and b_1 was close to 1.0 for all cases. The average power law exponent (b_2 in eq. (2)) was 2.8. This conforms closely with the exponent $b_2 = 2.6$ obtained when the short time solution to the diffusion problem (fig. 9) was fitted to equation (2). Thus, equation (1) with $n = 3$ is considered an adequate approximation for the short time solution, and the data were plotted as r/r_0 against $\left(t/r_0^2\right)^{1/3}$ in figure 8. In the case of internal pressure reentry simulation exposures and 1320° C, 1.33×10^1 N/m^2 exposure, the b_2 values deviated considerably from 2.6 which indicated that in these cases conditions assumed in the analytical solution do not strictly apply.

In all exposures FS-85 suffered greater interstitial contamination than Cb-752 (figs. 8(a) to (f)). On an average basis the extent of interstitial contamination was about 15 percent for FS-85.

In the 1320° C isobaric exposures, pressure played a very significant role in determining interstitial contamination as can be seen from comparison of the slopes in figures 8(a) and (b). In the 1320° C, 1.33×10^1 N/m^2 exposure little or no metal recession occurred and copious quantities of silicon oxide (SiO_2) were collected in the cold regions of the muffle indicating active silicide oxidation. These observations together with the small amount of interstitial contamination support a self-healing mechanism at 1320° C and 1.33×10^1 N/m^2 which accounts for the strong pressure effect observed between 1320° C isobaric exposures (figs. 8(a) and (b)).

The extent of interstitial contamination was relatively insensitive to pressure in the 1125° C exposures as can be seen from a comparison of slopes in figures 8(c) and (d). This is exactly what one would expect in the absence of a strong self-healing mechanism and if the oxide film exerts an insignificant resistance to oxygen ingress.

The effect of pressure on interstitial contamination was moderate in reentry simulation exposures as can be seen from a comparison of figures 8(e) and (f). This infers a weak self-healing effect.

The interstitial contamination data in table IV were used to compute apparent oxygen diffusivities D_a in the substrates for the various exposure conditions by using a short time solution for diffusion into a region bounded internally by a cylinder (ref. 8). The concentration term is

$$\frac{C - C_0}{C_s - C_0} \tag{3}$$

where C_0 is the initial oxygen content of the as-received sheet (table I), C_s the oxygen saturation concentration (as determined in the appendix), and C the oxygen concentration at KHN = 300 (fig. 7). Values of $\left(\sqrt{D_a t/r_0^2}\right)^{1/2}$ were determined from figure 9 for each r/r_0 value at the appropriate concentration. The majority of the $\left(\sqrt{D_a t/r_0^2}\right)^{1/2}$ values listed in table IV are below 2, which is the valid range for the short time solution of the diffusion problem. Higher values were determined by extrapolation. From $\left(\sqrt{D_a t/r_0^2}\right)^{1/2}$ and normalized exposure times, individual apparent oxygen diffusivities were computed. To get a best value for each alloy and exposure condition a least squares linear regression was performed for the cubic oxygen ingress model:

$$\frac{r}{r_0} = m_3\left(\frac{D_a t}{r_0^2}\right)^{1/3} + b_3 \tag{4}$$

using combined data for each alloy. The average regression coefficient was 0.995, which indicates a very good fit. Since equations (2) and (4) are of similar form, a best value of D_a can be computed for each alloy and exposure condition from

$$\overline{D}_a = \frac{m_1^3}{3600\, m_3^3} \tag{5}$$

For reentry simulation exposures, diffusivities were multiplied by 2 since each reentry cycle is equivalent to about 30 minutes at 1320° C. These diffusivities are listed in table V along with predicted diffusivities D_p (as determined in the appendix) and the ratio of apparent to predicted diffusivity D_a/D_p. In nearly all cases the ratio is less than 1. A value for this ratio of 0.1 or higher is considered good agreement between apparent and predicted values by the author since there is a spread factor of 20 in the published diffusion data used as a basis for predicting diffusivities. All of the diffusivity ratios for those exposures where no self-healing effect was noted fall above 0.1. The generally low values of these diffusivity ratios could be partially due to deviation from

the ideal behavior assumed in making the diffusivity predictions. In particular, the diffusivity of oxygen is probably depressed by the presence of zirconium. This effect is apparent when diffusivity ratios for FS-85 and Cb-752 are compared. Agreement between apparent and predicted diffusivities is generally better for FS-85 than for Cb-752. The zirconium content of FS-85 is lower than that of Cb-752. An additional reason for low diffusivity ratios may be deviation from the oxidation model - in particular, the columbium oxide formed at the defect may partially suppress oxygen ingress to the substrate in all cases.

For the 1320° C, 1.33×10^{1} N/m^2 exposures where a strong self-healing effect was observed, the diffusivity ratios were 5.1×10^{-4} and 2.0×10^{-3} for Cb-752 and FS-85, respectively. A considerably weaker self-healing process occurred during internal pressure reentry exposures. For this case the diffusivity ratios were 5.4×10^{-2} and 6.6×10^{-2} for Cb-752 and FS-85, respectively.

The important conclusions drawn from the results of this section are as follows:

(1) FS-85 suffered 15 percent greater average interstitial contamination than Cb-752.

(2) Self-healing occurred at 1.33×10^{1} N/m^2 (0.1 torr) and 1320° C and to a lesser extent under internal pressure reentry exposures based on the observed pressure sensitivity of interstitial contamination and small values of apparent to predicted diffusivity ratios.

(3) Interstitial contamination kinetics adhered closely to the short-time solution to the diffusion problem except where self-healing occurred.

Self-healing mechanism. - To obtain further insight into the oxidation and self-healing process at the defects, electron microprobe line scans were run in a radial direction from the defect center on several 0.028-centimeter FS-85 specimens. The elements columbium, oxygen, chromium, iron, and silicon were scanned. The results for reentry simulation exposed specimens are plotted in figure 10 as counts relative to the pure element standards against distance from the oxide-metal interface. Additional results are given in the last two columns of table V. One of the key factors in self-healing is the silicon content of the oxide. A comparison of the average silicon content of the oxide with the self-healing tendency as expressed by the diffusivity ratio (table V and fig. 11) shows that in the 1320° C exposures D_a/D_p decreases as the average silicon content increases. In the exposures where active oxidation occured, silicon was primarily transported to the defect through the gas phase. Although the low temperature exposures gave high silicon contents at the defect, self-healing did not occur in these specimens based on the high D_a/D_p ratios observed. In these exposures silicon was primarily transported to the defect by diffusion through the solid phases. The author attributes the difference in behavior between high and low temperature isobaric exposure to SiO_2 going into solution at elevated temperatures and precipitating as discrete oxide

particles at lower temperatures. A possible solvent for SiO_2 at temperatures above 1180° C is iron oxide (FeO) (ref. 6) which was, when detected as iron, always in proximity to silicon peaks.

In the specimen exposed to five external pressure reentry cycles, five major silicon peaks were found in the oxide at the defect (fig. 10(b)). In the specimen exposed for one cycle, a single major peak was found (fig. 10(a)). The locations of these peaks are plotted in figure 12 as functions of the square root of exposure cycles. The five peaks in the specimen exposed for five cycles lie along a straight line. Also, the first peak is about $(5)^{1/2}$ times the distance from the metal oxide interface as the peak in the specimen exposed for a single cycle. Thus, the positions of the silicon concentrations provide evidence that the metal recession reaction at the defects follows a parabolic rate equation. The silicon present in the oxide was probably deposited during the initial period of each cycle when the temperature was high and the oxygen partial pressure was low.

SUMMARY OF RESULTS

The purpose of this study was to examine the kinetics of defect growth and interstitial contamination at a nominal 0.08-centimeter hole through fused slurry silicide coated FS-85 and Cb-752 specimens. A second purpose was to determine the mechanism and extent of self-healing at the defect site. The defected coupons were exposed to either isothermal isobaric exposures at 1.33×10^{1} or 1.33×10^{3} N/m^2 (0.1 or 10 torr) and 1125° or 1320° C, or to internal or external pressure reentry simulation exposures. Metal recession and interstitial contamination were followed by metallographic and microhardness measurements. Supplemental weight change measurements on the oxidized specimens, XRD analysis of the oxides formed on the coatings, XRD and spectrochemical analyses of vaporized oxides, and EMP scans of the defected region were performed to obtain a fuller understanding of self-healing processes occurring at the defect.

The following are the results of this study:

1. In isothermal exposures at 1320° C and 1.33×10^{3} N/m^2, the metal recession for FS-85 was about 15 percent greater than for Cb-752, whereas in five external pressure reentry simulation cycles the metal recession for these alloys was about the same with the defect only growing from about 0.08 to 0.12 centimeter in diameter.

2. The average rate of interstitial contamination was about 15 percent greater for FS-85 than for Cb-752. In five external pressure reentry cycles the radius of the interstitially contaminated zone was only three to four times that of the initial defect (contamination of an area about 0.24 to 0.32 cm in diameter).

3. Self-healing occurred in the 1320° C, 1.33×10^{1} N/m^2 (0.1 torr) exposures and to a lesser extent in internal pressure reentry exposures.

4. For self-healing to occur, large amounts of silicon must be deposited at the coating defect as a result of active oxidation of the silicide coatings.

5. With the exception of exposures where boundary conditions were altered by self-healing, the kinetics of interstitial contamination at through-hole defects in coated columbium alloys adhered closely to an available short-time diffusion analysis (for an infinite medium bounded internally by a cylindrical source).

Lewis Research Center,
National Aeronautics and Space Administration,
and
U. S. Army Air Mobility R&D Laboratory,
Cleveland, Ohio, April 3, 1973,
501-21.

APPENDIX - BACKGROUND IN DEFECT GROWTH AND INTERSTITIAL CONTAMINATION

Theory

In the temperature and pressure range of interest for reentry vehicles, 900^{o} to 1400^{o} C and 1.33×10^{1} to 4×10^{3} N/m^{2}, columbium initially oxidizes in a parabolic manner (ref. 7). At the outset, oxygen is present as an interstitial in the metal. Then CbO and CbO_2 are formed at the metal-atmosphere interface and parabolic kinetics are observed. After a period of time Cb_2O_5 is formed and the oxidation rate becomes linear. The length of the dissolution and parabolic oxidation periods are a function of temperature and oxygen pressure. As the temperature or pressure is increased these periods become shorter.

From knowledge of diffusivity data, one should also be able to estimate the amount of interstitial oxygen ingress. Procedures for making this estimate are now presented.

Oxygen Contamination

Diffusivities for oxygen in columbium have been determined by relaxation, internal friction, and oxygen gradient techniques. Some results are presented in Kofstad (ref. 7). The average oxygen diffusivity in columbium based on all three methods is 2.4×10^{-6} square centimeter per second at 1125^{o} C and 9.5×10^{-6} square centimeter per second at 1320^{o} C. The spread in the data is about one order of magnitude. The diffusivities of oxygen in each of the alloying elements (ref. 7) and the adjusted oxygen diffusivities for FS-85 and Cb-752 assuming ideal solution behavior are listed in table VI. Note that the corrections to the values for unalloyed columbium are relatively small compared to the uncertainties in the diffusivity data for the alloying elements.

Prediction of oxygen ingress is considerably more complex. A strictly rigorous treatment of the problem is beyond the scope of this report. Kofstad (ref. 7) presents a solution for simultaneous growth of an oxide film on a flat, semi-infinite metal with oxygen dissolution occurring in the underlying metal. Although neither the assumptions nor the flat plate geometry are applicable, a useful criterion is developed which may be applied to the problem of interest. When $S << (Dt)^{1/2}$ (where S is the metal recession, D the oxygen diffusivity in the substrate, and t the time) oxygen penetration of the substrate is, to a good approximation, independent of transport processes in the oxide film. This is the case for the problem of interest based on expected metal recessions and predicted oxygen diffusivities in the substrates. Additional statements are implied:

(1) Oxide formation causes negligible motion of the metal oxide boundary.

(2) The concentration of oxygen at the metal oxide boundary is constant.

(3) As developed previously, oxygen penetration is primarily a function of diffusion in the metal. That is, resistance to oxygen ingress through the oxide is negligible and no self-healing mechanism is operative.

For the previous conditions, Crank (ref. 8) presents a solution applicable for short times in the region $r > r_0$:

$$\frac{C - C_0}{C_s - C_0} = \left(\frac{r_0}{r}\right)^{1/2} \operatorname{erfc} \frac{r - r_0}{2\sqrt{Dt}} + \frac{(r - r_0)(Dt)^{1/2}}{4r_0^{1/2}r^{3/2}} \operatorname{ierfc} \frac{r - r_0}{2\sqrt{Dt}}$$

$$+ \frac{Dt\left(9r_0^2 - 2r_0r - 7r^2\right)}{32r_0^{3/2}r^{5/2}} i^2\operatorname{erfc} \frac{r - r_0}{2\sqrt{Dt}} + \ldots$$

Solutions to the equation are plotted by Crank. They are crossplotted in figure 9. With an estimate of $(C - C_0)/(C_s - C_0)$ and the diffusivity of oxygen in columbium in hand, one may use this figure to estimate oxygen penetration, or one may use oxygen penetration data to estimate apparent oxygen diffusivities. The latter procedure is followed in this report.

For pure columbium the microhardness H is related to oxygen concentration by

$$H = b + kC \tag{9}$$

over relatively small concentration intervals. For a getter containing alloy, a linear relation can be applied for each heat treatment condition. Since C_0 is known and C_s can be estimated, only C need be determined from microhardness data.

Data are not available for the solubility of oxygen in FS-85 and Cb-752. Therefore, estimates were made from data for the solubilities of oxygen (O) in columbium (Cb), tantalum (Ta), zirconium (Zr), and tungsten (W) found in Shunk (ref. 10) and Elliott (ref. 11). Based on the data in Shunk for the Cb-O system and in Elliott for the Ta-O system, the solubility of O in Nb rich Cb-Ta solid solutions is approximately equal to the solubility of O in pure Cb. At 1125° C the solubility is 3.0 atom percent and at 1320° C it is 4.0 atom percent. The solid solubility of O in W is reported to be 0.06 atom percent at 1700° C (ref. 11). The solid solubility of O in Zr is 2.8 atom percent at 1125° C and 5.0 atom percent at 1320° C (ref. 11). Assuming ideal solid solutions between alloys of (Cb, Ta) and W and (Cb, Ta) and Zr permits an estimation of the solid solubility of O in FS-85 and Cb-752 to be made. Zirconium exerts less than a 0.1-atom percent influ-

ence at the concentrations of interest. Based on the influence of W alone, the solid solubility of oxygen in FS-85 is estimated to be 3.8 atom percent at 1320° C and 2.8 atom percent at 1125° C. For Cb-752 the solid solubility is 3.7 atom percent at 1320° C and 2.8 atom percent at 1125° C. Microhardness against interstitial oxygen concentration data were obtained experimentally for FS-85 only. The results are discussed in the text. The microhardness-concentration relation for Cb-752 is assumed to be the same as for FS-85. At KHN_{200g} = 300, C was determined from the microhardness-concentration plot in figure 7.

REFERENCES

1. Grisaffe, S. J.; Merutak, J. P.; and Levine, S. R.: A Status Review of Lewis Research Center Supported Protection System Development. NASA TM X-52977, 1971.

2. Burford, J. C.; Johnson, C. E.; and Ong, C. C.: The Effect of the Meteroid Environment on a Coated Columbium Radiative Heat Shield for a Space Shuttle. Rep. TM-70-1012-1, Bellcomm, Inc. (NASA CR-116541), Apr. 17, 1970.

3. Bartlett, E. S.; Maykuth, D. J.; Grinberg, I. M.; and Luce, B. G.: Degradation and Reverse of Radiative-Thermal-Protection-System Materials for the Space Shuttle. NASA CR-123972, 1972.

4. Barrett, Charles A.: Controlled Oxygen Additions to Refractory Metals. NASA TM X-1799, 1969.

5. Stoner, D. R.: Determination of Weldability and Elevated Temperature Stability of Refractory Metal Alloys. III - Effect of Contamination Level on Weldability of Refractory Metal Alloys. NASA CR-1609, 1970.

6. Levin, Ernest M.: Robbins, C. R.; and McMurdie, H. F.: Phase Diagrams for Ceramists. American Ceramic Soc., 1964.

7. Kofstad, Per: High-Temperature Oxidation of Metals. John Wiley & Sons, Inc., 1966.

8. Crank, John: The Mathematics of Diffusion. Oxford University Press, 1956, pp. 82-83.

9. Klopp, William D.; Sims, Chester T.; and Jaffee, Robert I.: High-Temperature Oxidation and Contamination of Columbium. Trans. ASM, vol. 51, 1959, pp. 282-298.

10. Shunk, Francis A.: Constitution of Binary Alloys, Second Supplement. McGraw-Hill Book Co., Inc., 1969.

11. Elliott, Rodney P.: Constitution of Binary Alloys, First Supplement. McGraw-Hill Co., Inc., 1965.

12. Gentry, W. O.; and Michael, A. B.: Properties of Some Columbium-Rich Alloys in The Columbium-Tantalum-Tungsten-Zirconium System. High-Temperature Materials II. G. M. Ault, W. F. Barclay, and H. P. Munger, eds, Interscience Publ., 1963, pp. 307-324.

13. Michael, A. B.: The Oxidation of Columbium-Base and Tantalum-Base Alloys. Reactive Metals. W. R. Clough, ed. Interscience Publ., 1959, pp. 487-507.

TABLE I. - ANALYSIS OF Cb-752 AND FS-85

Element	Cb-752 Wah Chang heat 770022	FS-85 Fansteel heat 85D2577
Interstitial content of as-received sheet, ppm		
O	180	245
C	40	130
N	50	30
H	4	3
Ingot analysis, composition in weight percent		
Ta	0.4	27.6
W	9.1	10.6
Zr	2.7	.94
Cb	bal	bal
Ingot analysis, impurity content, ppm		
Al	<20	[a]NA
C	60	NA
Cd	5	40
Co	<10	NA
Cr	<20	NA
Fe	<50	<50
H	7	<5
Hf	440	<100
Mg	<20	NA
Mn	<20	NA
Mo	130	<100
N	50	30
Ni	<20	NA
O	140	40
Pb	<20	NA
Si	<50	<50
Sn	15	NA
Ti	<40	<50
V	<20	NA

[a]NA, element not analyzed.

TABLE II. - COATING AND ALLOY DATA

Substrate	Initial substrate thickness, cm	Knoop hardness number (as-received sheet)	Coating	Nominal coating composition	Coating weight, mg/cm^2	Coating thickness, cm/side	Coated substrate thickness, cm	Knoop hardness number (as-coated sheet), KHN_{200g}
Cb-752	0.033	185	VH-109	Si, Hf, Ta+Si, Hf, Cr, Fe	25	0.0078	0.027	150
Cb-752	.033	185	R512E	Si-20Cr-20Fe	24	0076	.025	150
FS-85	.028	220	R512E	Si-20Cr-20Fe	25	.0082	.022	165
FS-85	.033	220	R512E	Si-20Cr-20Fe	25	.0082	.028	165

TABLE III. - IN SITU METALLOGRAPHIC AND X-RAY DIFFRACTION ANALYSES OF OXIDES FORMED ON FUSED SLURRY SILICIDE COATED Cb-752 AND FS-85 AFTER 5 CYCLES AT 1320° C REENTRY SIMULATION EXPOSURE

Coating	Substrate	Exposure pressure	Oxide thickness, cm	Oxide appearance under polarized light	Oxide phases detected by X-ray diffraction
R512E	Cb-752	External	0.016	White, rust, SiO_2	Cb_2O_5, $(Fe,Cr)CbO_4$
R512E	Cb-752	Internal	.002	White, blue, rust	Cb_2O_5, $(Fe,Cr)CbO_4$, $(M)WO_4$
R512E	FS-85	External	.019	White, blue, rust	Cb_2O_5, $(Fe,Cr)CbO_4$
R512E	FS-85	Internal	.002	White	Cb_2O_5, $(Fe,Cr)CbO_4$
VH-109	Cb-752	External	.007	White, green, tan	HfO_2, $HfSiO_4$, Cr_2O_3
VH-109	Cb-752	Internal	.002	White, green, tan	HfO_2, $(Fe,Cr)CbO_4$, Cr_2O_3

TABLE IV. - SUMMARY OF METALLOGRAPHIC DATA FOR DEFECTED AND EXPOSED FUSED SLURRY SILICIDE COATED FS-85 AND Cb-752

Alloy	Coating	Initial defect radius, r_0, cm	Normalized exposure time, $t^{1/2}/r_0$, $\frac{hr^{1/2}}{cm}$	Metal recession, Δr, cm	Normalized radius of contaminated zone, r/r_0, cm/cm	Concentration, $\frac{C - C_0}{C_s - C_0}$	$\sqrt{\frac{D_a t}{r_0^2}}$	Apparent diffusivity of oxygen, D_a, cm^2/sec
Exposure at 1320° C, 1.33×10^3 N/m^2, 1 hr								
0.028 FS-85	R512E	0.040	25.0	0.018	2.92	0.34	2.22	2.2×10^{-6}
0.033 FS-85	R512E	.044	22.7	.018	2.68	.34	1.89	1.9
Cb-752	R512E	.049	20.4	.018	2.55	.36	1.79	2.1
Cb-752	VH-109	.043	23.3	.015	2.62	.36	1.81	1.7
Exposure at 1320° C, 1.33×10^3 N/m^2, 5 hr								
0.028 FS-85	R512E	0.037	60.4	0.041	5.60	0.34	5.48	2.3×10^{-6}
0.033 FS-85	R512E	.049	45.6	.030	4.31	.34	4.10	2.2
Cb-752	R512E	.041	54.5	.025	3.80	.36	3.63	1.2
Cb-752	VH-109	.036	62.1	.036	4.24	.36	4.20	1.3
Exposure at 1320° C, 1.33×10^1 N/m^2, 1 hr								
0.028 FS-85	R512E	0.039	25.6	~0	1.41	0.34	0.39	6.4×10^{-8}
0.033 FS-85	R512E	.042	23.8	↓	1.29	.34	.32	5.0
Cb-752	R512E	.044	22.7	↓	1.18	.36	.22	2.6
Cb-752	VH-109	.044	22.7	↓	1.11	.36	.17	1.6
Exposure at 1320° C, 1.33×10^1 N/m^2, 5 hr								
0.028 FS-85	R512E	0.046	48.6	~0	1.26	0.34	0.28	9.2×10^{-9}
0.033 FS-85	R512E	.049	45.6	↓	1.57	.34	.50	3.3×10^{-8}
Cb-752	R512E	.044	50.8	↓	1.27	.36	.30	9.7×10^{-9}
Cb-752	VH-109	.043	52.0	↓	1.12	.36	.17	3.0×10^{-9}

TABLE IV. - Continued. SUMMARY OF METALLOGRAPHIC DATA FOR DEFECTED AND EXPOSED FUSED SLURRY SILICIDE COATED FS-85 AND Cb-752

Alloy	Coating	Initial defect radius, r_0, cm	Normalized exposure time, $t^{1/2}/r_0$, $\frac{hr^{1/2}}{cm}$	Metal recession, Δr, cm	Normalized radius of contaminated zone, r/r_0, cm/cm	Concentration, $\frac{C - C_0}{C_s - C_0}$	$\sqrt{\frac{D_a t}{r_0^2}}$	Apparent diffusivity of oxygen, D_a, cm^2/sec
Exposure at 1125° C, 1.33×10^3 N/m^2, 1 hr								
0.028 FS-85	R512E	0.045	22.2	0.009	2.65	0.48	3.11	5.4×10^{-6}
0.033 FS-85	R512E	.044	22.7	.010	2.73	↓	3.29	5.8
Cb-752	R512E	.044	22.7	.012	2.48	↓	2.66	3.8
Cb-752	VH-109	.046	21.7	.010	2.24	↓	2.12	2.6
Exposure at 1125° C, 1.33×10^3 N/m^2, 5 hr								
0.028 FS-85	R512E	0.044	50.8	0.015	3.64	0.48	5.39	3.1×10^{-6}
0.033 FS-85	R512E	.046	48.6	.011	3.52	↓	4.86	2.8
Cb-752	R512E	.039	57.3	.020	3.57	↓	4.97	2.1
Cb-752	VH-109	.045	49.7	.023	3.33	↓	4.53	2.3
Exposure at 1125° C, 1.33×10^1 N/m^2, 1 hr								
0.028 FS-85	R512E	0.044	22.7	~0	2.39	0.48	2.46	3.3×10^{-6}
0.033 FS-85	R512E	.055	18.2	↓	2.22	↓	2.06	3.6
Cb-752	R512E	.039	25.6	↓	2.12	↓	1.85	1.5
Cb-752	VH-109	.037	27.0	↓	1.92	↓	1.41	5.4×10^{-7}
Exposure at 1125° C, 1.33×10^{-1} N/m^2, 5 hr								
0.028 FS-85	R512E	0.045	49.7	~0	3.56	0.48	4.95	2.8×10^{-6}
0.033 FS-85	R512E	.043	52.0	.001	3.44	↓	4.72	2.3
Cb-752	R512E	.044	50.8	.001	2.52	↓	2.79	8.4×10^{-7}
Cb-752	VH-109	.039	57.3	.002	2.64	↓	3.08	8.0

TABLE IV. - Concluded. SUMMARY OF METALLOGRAPHIC DATA FOR DEFECTED AND EXPOSED FUSED SLURRY SILICIDE COATED FS-85 AND Cb-752

Alloy	Coating	Initial defect radius, r_0, cm	Normalized exposure time, $t^{1/2}/r_0$, $\frac{cycles^{1/2}}{cm}$	Metal recession, Δr, cm	Normalized radius of contaminated zone, r/r_0, cm/cm	Concentration, $\frac{C - C_0}{C_s - C_0}$	$\sqrt{\frac{D_a t}{r_0^2}}$	Apparent diffusivity of oxygen, D_a, cm^2/sec[a]
Exposure for 1 external pressure reentry cycle								
0.028 FS-85	R512E	0.044	22.7	0.009	1.86	0.34	0.78	6.5×10^{-7}
0.033 FS-85	R512E	.053	18.9	.010	2.34	.34	1.41	3.1×10^{-6}
Cb-752	R512E	.049	20.4	.010	1.94	.36	.95	1.2
Cb-752	VH-109	.040	25.0	.007	2.40	.36	1.60	2.3
Exposure for 5 external pressure reentry cycles								
0.028 FS-85	R512E	0.038	58.8	0.017	2.95	0.34	2.28	8.3×10^{-7}
0.033 FS-85	R512E	.041	54.5	.016	4.03	.34	3.69	2.5×10^{-6}
Cb-752	R512E	.042	53.2	.017	3.34	.36	2.96	1.7
Cb-752	VH-109	.043	52.0	.025	3.05	.36	2.56	1.3
Exposure for 1 internal pressure reentry cycle								
0.028 FS-85	R512E	0.040	25.0	~0	1.42	0.34	0.39	1.4×10^{-7}
0.033 FS-85	R512E	.048	20.8	↓	1.87	.34	.81	8.4
Cb-752	R512E	.045	22.2	↓	1.73	.36	.67	5.1
Cb-752	VH-109	.052	19.2	↓	1.25	.36	.29	1.3
Exposure for 5 internal pressure reentry cycles								
0.028 FS-85	R512E	0.043	52.0	~0	2.12	0.34	1.10	2.5×10^{-7}
0.033 FS-85	R512E	.065	40.7	↓	2.85	.34	2.12	2.1×10^{-6}
Cb-752	R512E	.037	60.4	↓	2.97	.36	2.42	8.9×10^{-7}
Cb-752	VH-109	.047	47.6	↓	2.10	.36	1.18	3.4

[a] D_a values were multiplied by 2 since each cycle is equivalent to about 30 minutes at 1320° C.

TABLE V. - COMPARISON OF PREDICTED AND APPARENT DIFFUSIVITIES OF OXYGEN IN FS-85 AND Cb-752

Alloy	Temperature, ^{o}C	Pressure, N/m^2	Apparent diffusivity, $\overline{D}_a$, cm^2/sec	Predicted diffusivity, D_p, cm^2/sec	$\frac{\overline{D}_a}{D_p}$	Average silicon concentration, percent (a)	Average iron concentration, percent (a)
FS-85	1320	1.33×10^{3}	2.2×10^{-6}	9.5×10^{-6}	2.3×10^{-1}	1.0	0
Cb-752	↓	1.33×10^{3}	1.3×10^{-6}	1.1×10^{-5}	1.2×10^{-1}	---	---
FS-85	↓	1.33×10^{1}	1.9×10^{-8}	9.5×10^{-6}	2.0×10^{-3}	4.5	.5
Cb-752	↓	1.33×10^{1}	5.6×10^{-9}	1.1×10^{-5}	5.1×10^{-4}	---	---
FS-85	1125	1.33×10^{3}	3.2×10^{-6}	2.6×10^{-6}	1.2	3.1	1.2
Cb-752	↓	1.33×10^{3}	2.3×10^{-6}	2.7×10^{-6}	8.5×10^{-1}	---	---
FS-85	↓	1.33×10^{1}	2.6×10^{-6}	2.6×10^{-6}	1.0	2.5	0
Cb-752	↓	1.33×10^{1}	8.5×10^{-7}	2.7×10^{-6}	3.1×10^{-1}	---	---
FS-85	1320	External	[b] 1.3×10^{-6}	9.5×10^{-6}	1.4×10^{-1}	.3	.2
Cb-752	↓	External	[b] 1.6×10^{-6}	1.1×10^{-5}	1.5×10^{-1}	---	---
FS-85	↓	Internal	[b] 6.3×10^{-7}	9.5×10^{-6}	6.6×10^{-2}	3.3	.5
Cb-752	↓	Internal	[b] 5.9×10^{-7}	1.1×10^{-5}	5.4×10^{-2}	---	---

[a] Percent relative to pure element standards.

[b] D_a values were multiplied by 2 since each cycle is equivalent to about 30 minutes at 1320^{o} C.

TABLE VI. - OXYGEN DIFFUSIVITIES IN THE ALLOYING ELEMENTS AND PREDICTED DIFFUSIVITIES FOR FS-85 AND Cb-752

Metal	Diffusivities at 1125° C, cm^2/sec	Diffusivities at 1320° C, cm^2/sec
Literature values		
Cb	2.4×10^{-6}	9.5×10^{-6}
Ta	7.2×10^{-7}	2.3×10^{-6}
W	2.3×10^{-6}	6.5×10^{-4}
Zr (zircaloy-2)	7.4×10^{-8}	4.5×10^{-7}
Predicted values		
FS-85	2.6×10^{-6}	9.5×10^{-6}
Cb-752	2.7×10^{-6}	1.1×10^{-5}

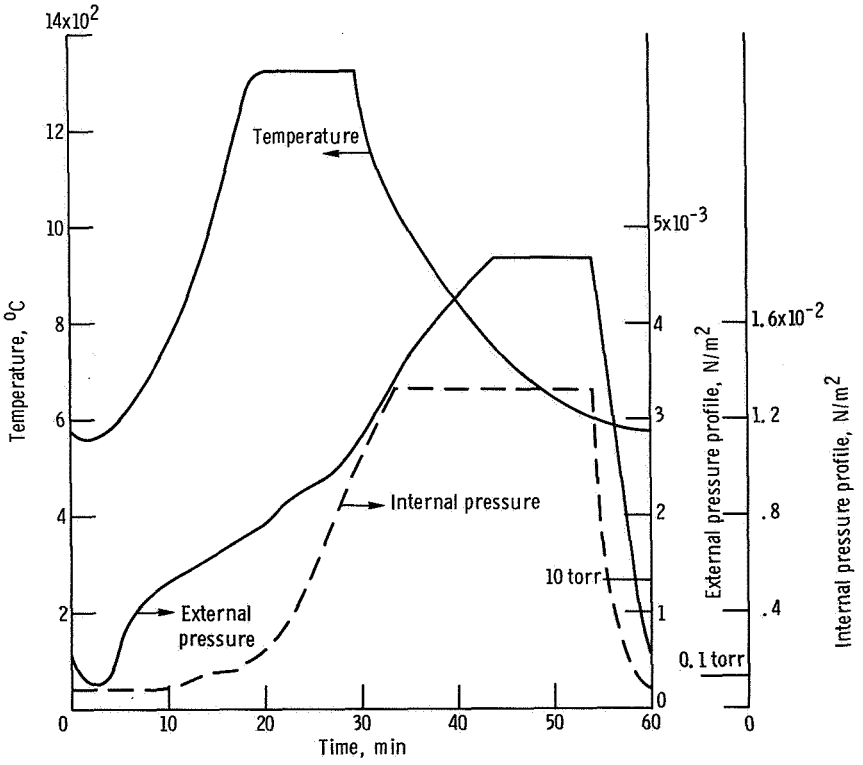

Figure 1. - Typical reentry simulation exposure profile.

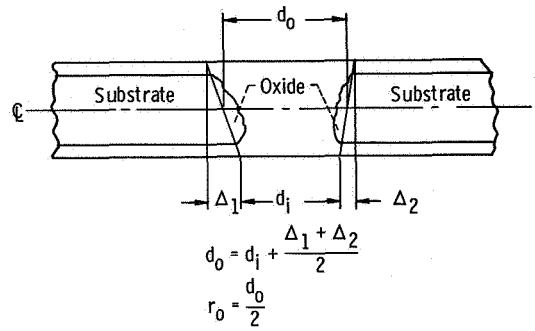

Figure 2. - Procedure for calculating initial defect diameter. Initial diameter of defect on substrate centerline, d_0; initial minimum diameter of defect from optical comparator, d_i; filar micrometer measurements of slopes after exposure, Δ_i.

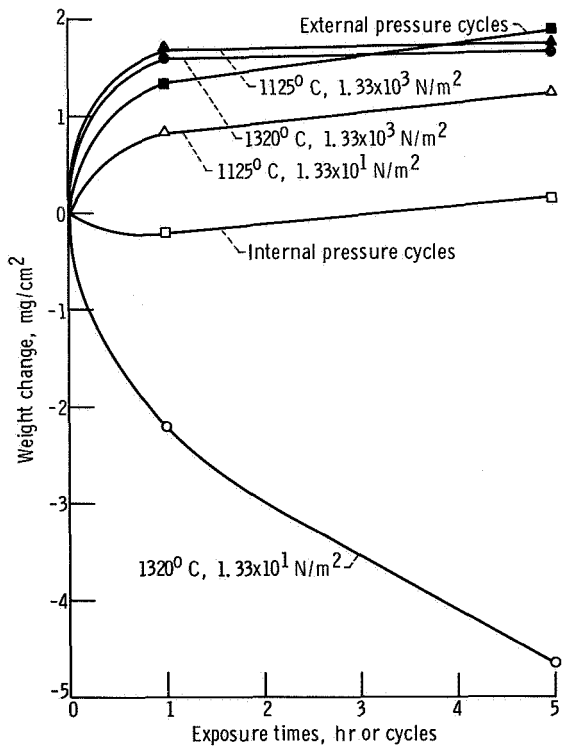

Figure 3. - Typical weight change behavior of fused slurry silicide coated columbium - R512E on FS-85.

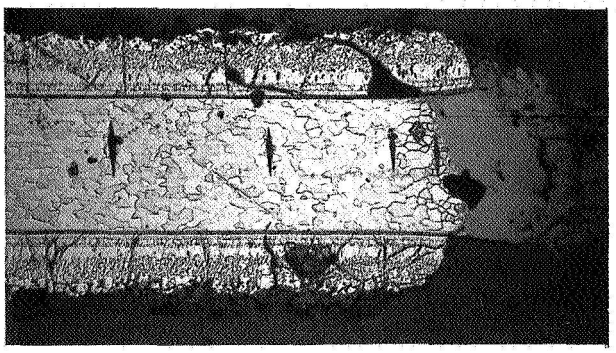

(a) Exposure: 1320^0 C, 1.33×10^3 newtons per square meter, 1 hour.

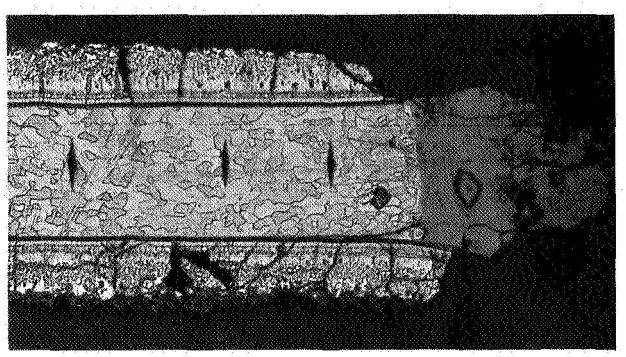

(b) Exposure: 1320^0 C, 1.33×10^3 newtons per square meter, 5 hours.

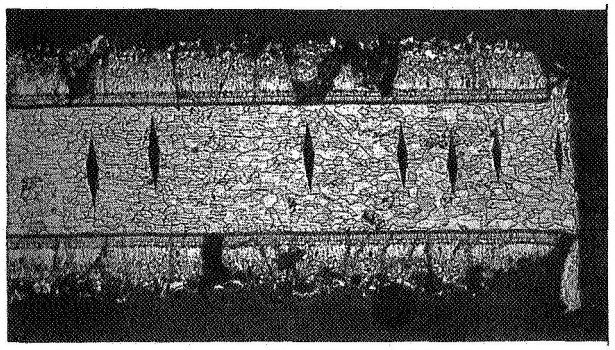

(c) Exposure: 1320^0 C, 1.33×10^1 newtons per square meter, 1 hour.

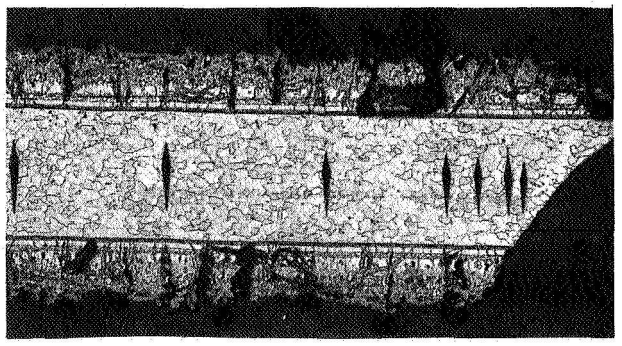

(d) Exposure: 1320^0 C, 1.33×10^1 newtons per square meter, 5 hours.

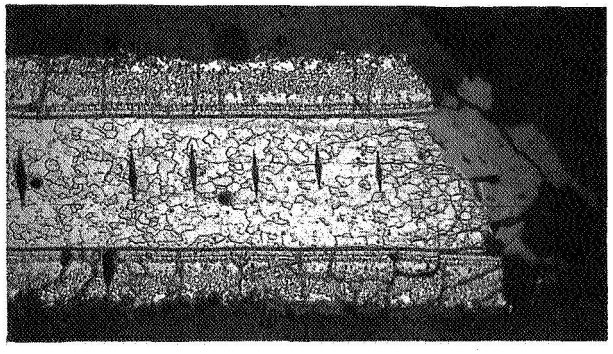

(e) Exposure: 1125^0 C, 1.33×10^3 newtons per square meter, 1 hour.

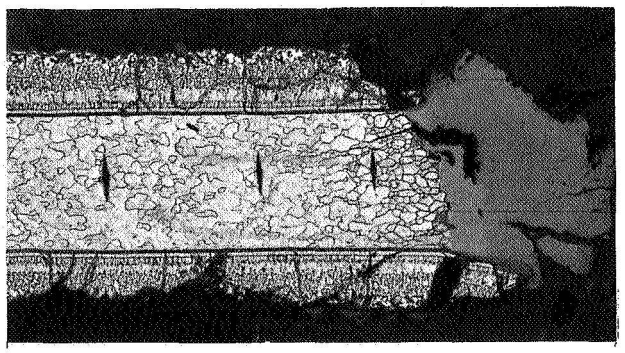

(f) Exposure: 1125^0 C, 1.33×10^3 newtons per square meter, 5 hours.

Figure 4. - Photomicrographs of section through defect in R512E coated FS-85 after exposure. X100.

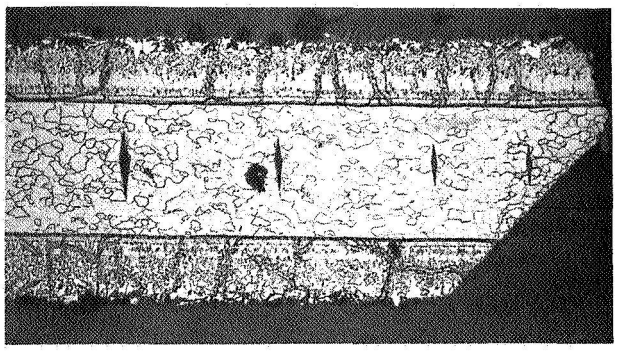

(g) Exposure: 1125^{0} C, 1.33×10^{1} newtons per square meter, 1 hour.

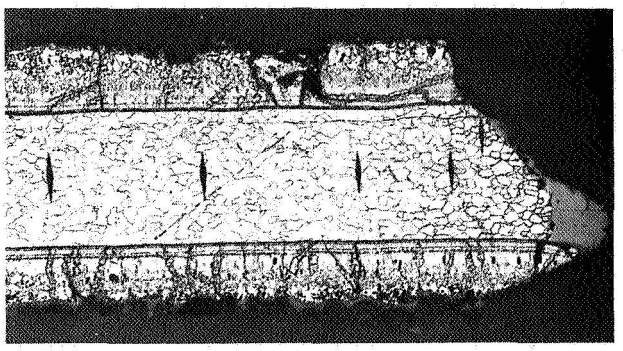

(h) Exposure: 1125^{0} C, 1.33×10^{1} newtons per square meter, 5 hours.

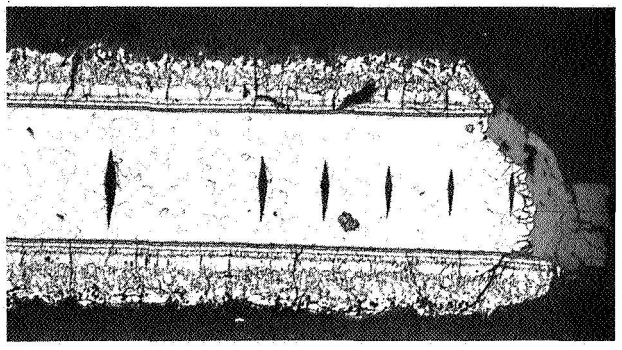

(i) Exposure: one external pressure reentry simulation cycle.

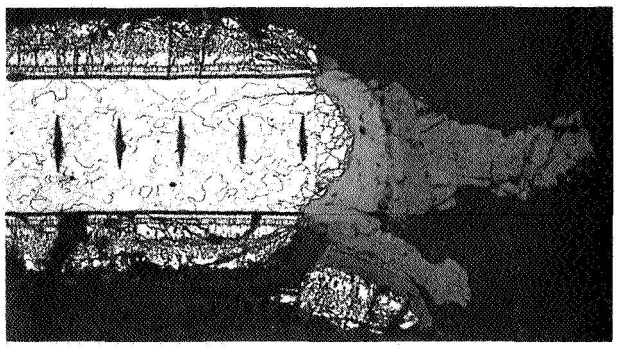

(j) Exposure: five external pressure reentry simulation cycles.

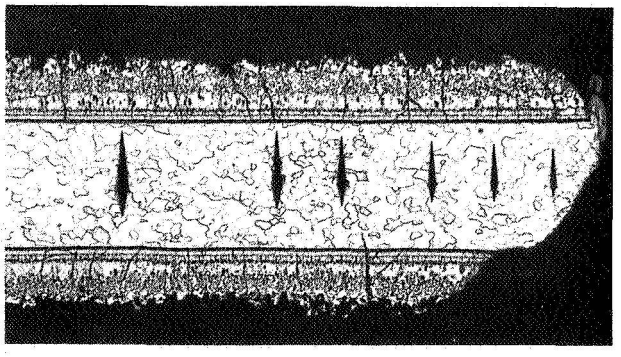

(k) Exposure: one internal pressure reentry simulation cycle.

(l) Exposure: five internal pressure reentry simulation cycles.

Figure 4. - Concluded.

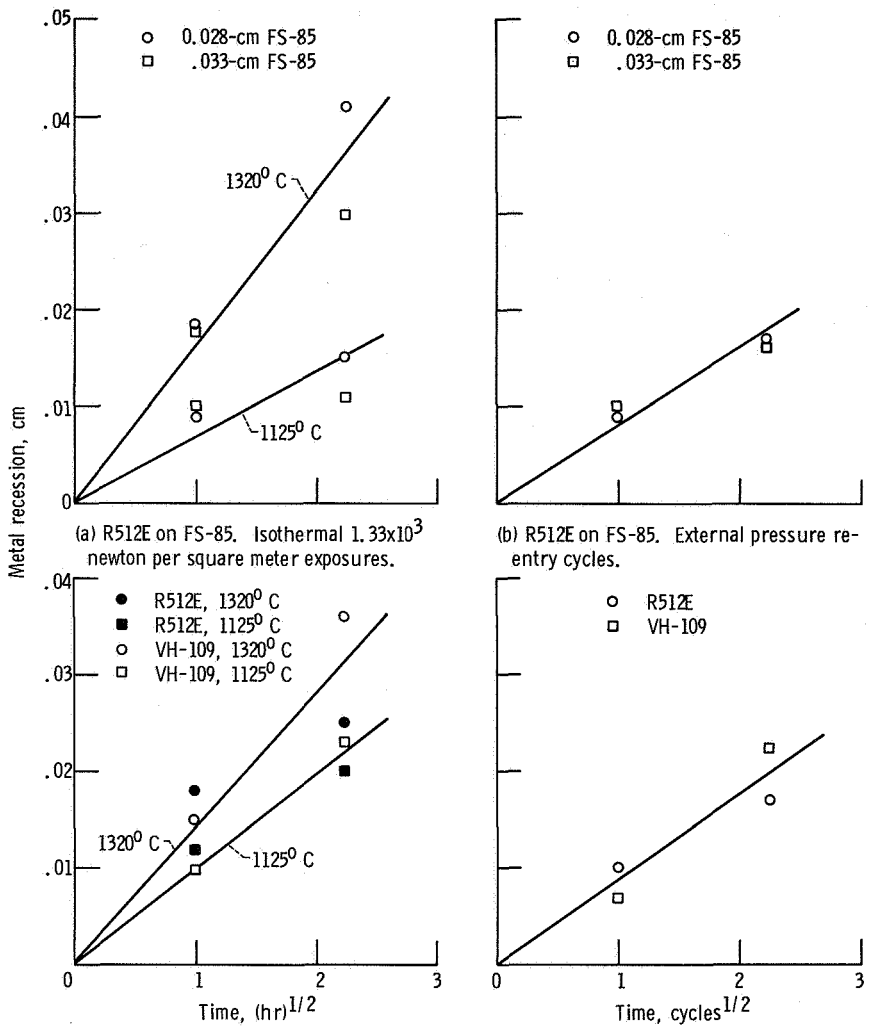

(a) R512E on FS-85. Isothermal 1.33×10^3 newton per square meter exposures.

(b) R512E on FS-85. External pressure reentry cycles.

(c) R512E and VH-109 on Cb-752. Isothermal 1.33×10^3 newton per square meter exposures.

(d) R512E and VH-109 on Cb-752. External pressure reentry cycles.

Figure 5. - Radial metal recession at through-hole defects in fused slurry sililide coated FS-85 and Cb-752.

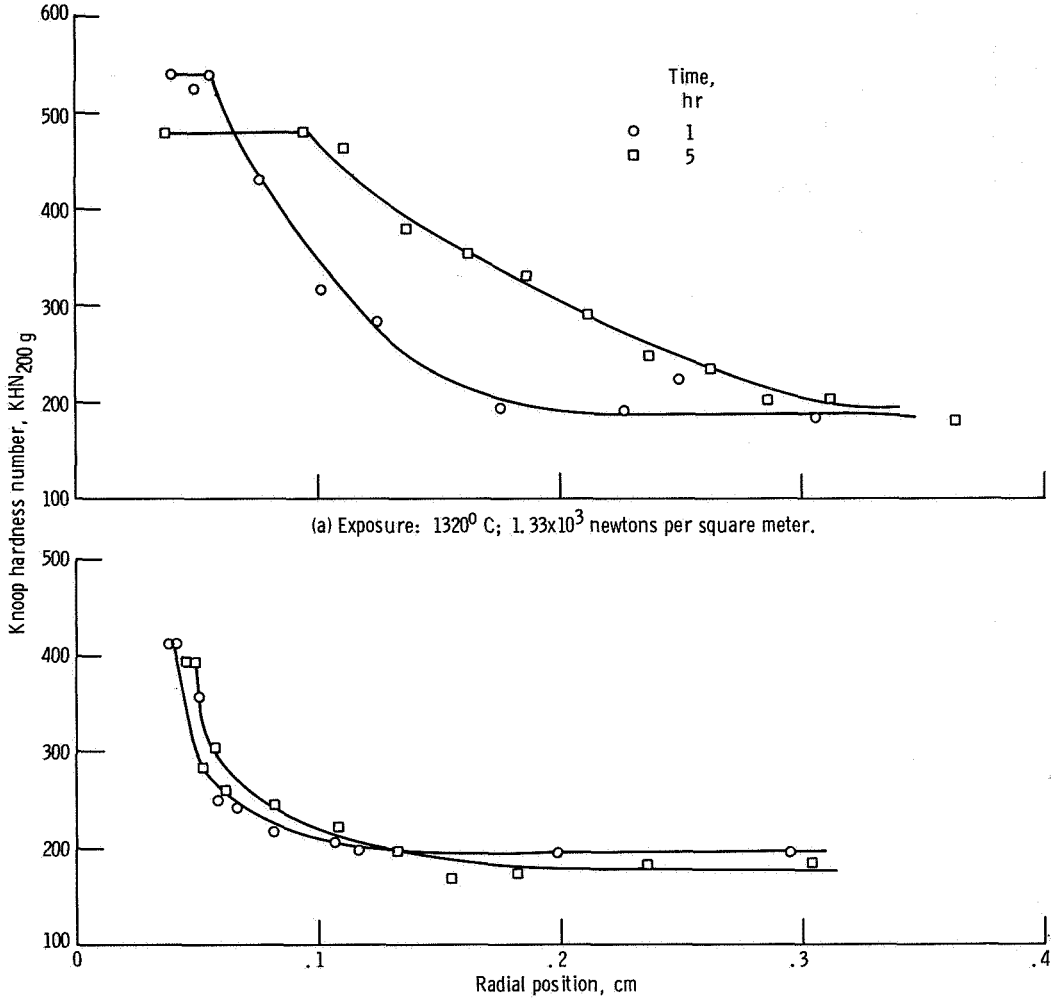

(a) Exposure: 1320^0 C; 1.33×10^3 newtons per square meter.

(b) Exposure: 1320^0 C; 1.33×10^1 newtons per square meter.

Figure 6. - Microhardness traverses of 0.028-centimeter R512E coated FS-85 in radial direction from center of 0.08-centimeter diameter defect after exposure.

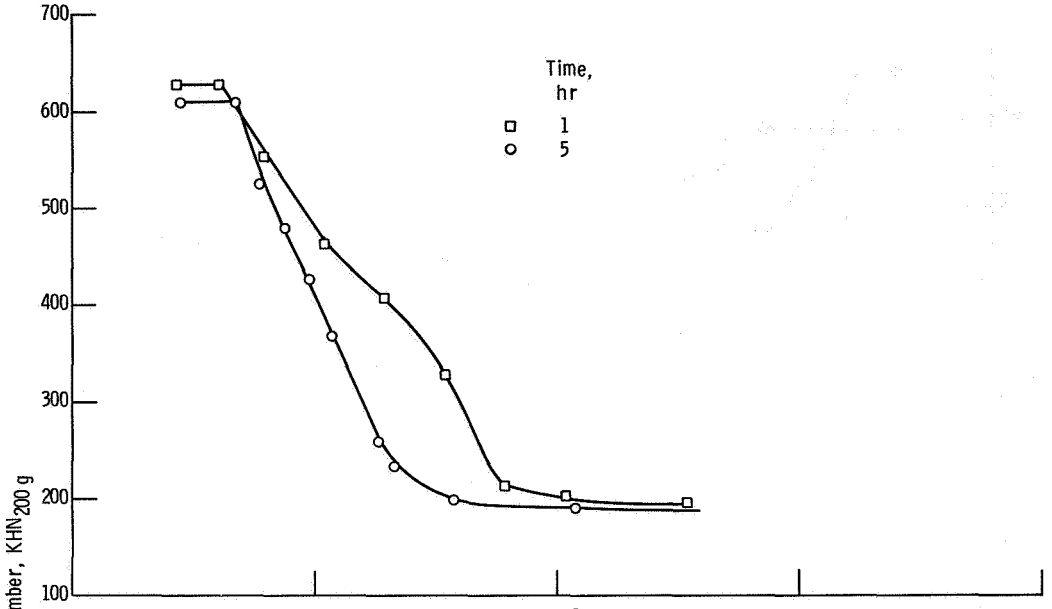

(c) Exposure: 1125° C; 1.33×10^3 newtons per square meter.

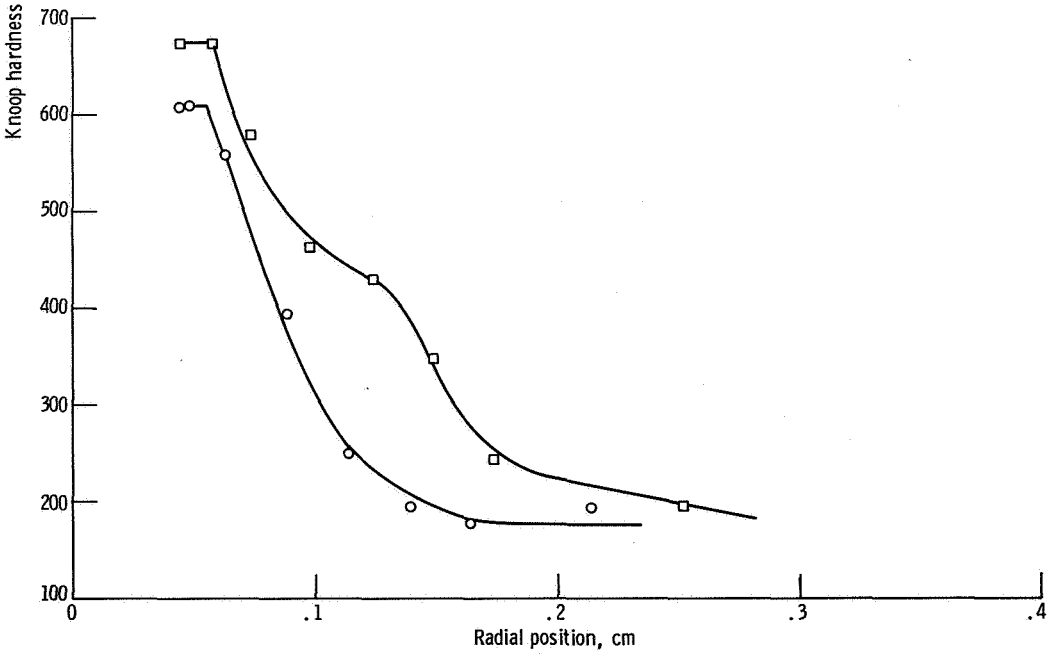

(d) Exposure: 1125° C; 1.33×10^1 newtons per square meter.

Figure 6. - Continued.

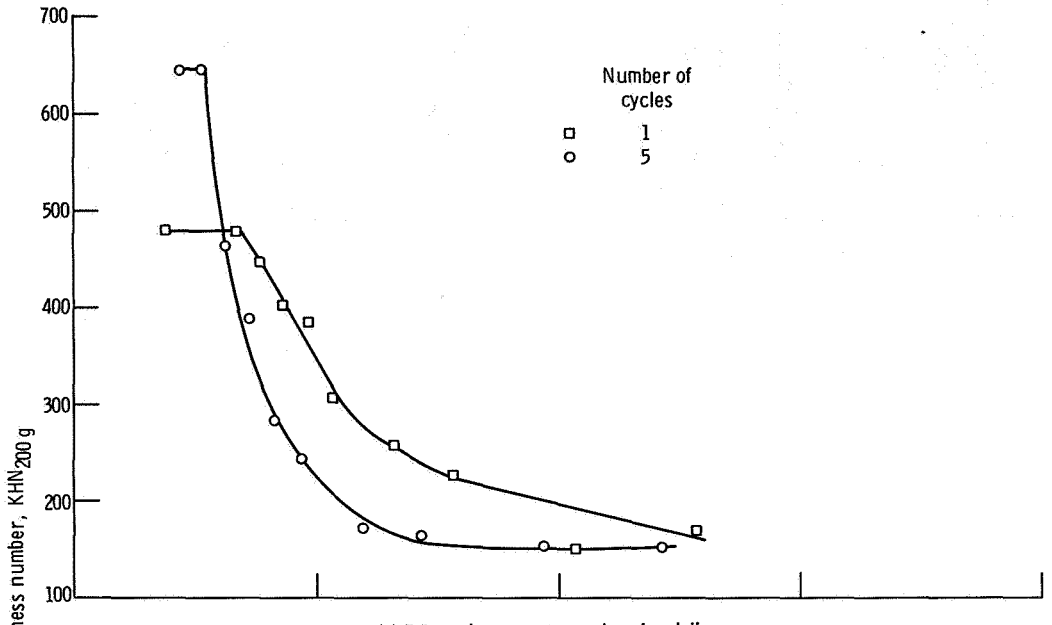

(e) External pressure reentry simulation.

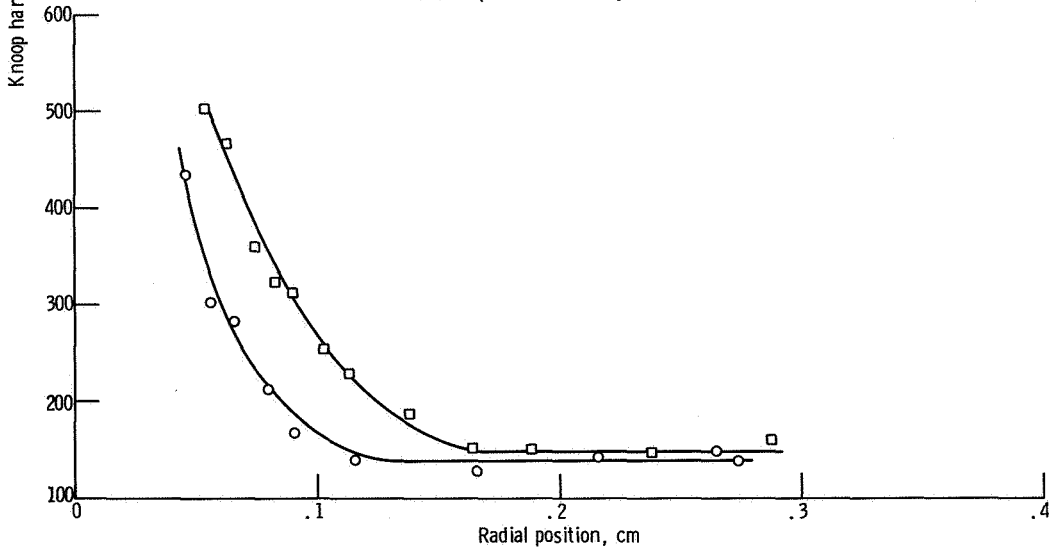

(f) Internal pressure reentry simulation.

Figure 6. - Concluded.

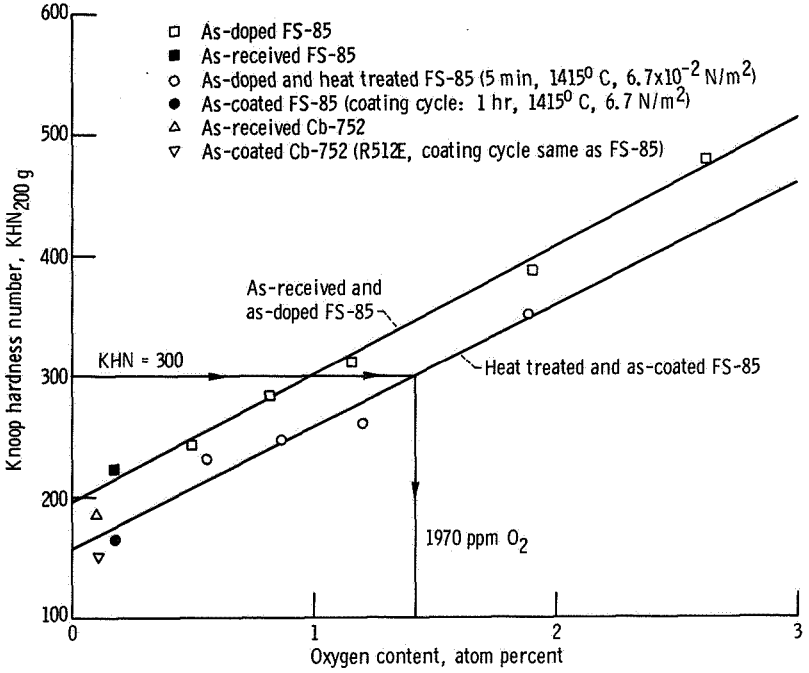

Figure 7. - Knoop microhardness as function of oxygen content for FS-85.

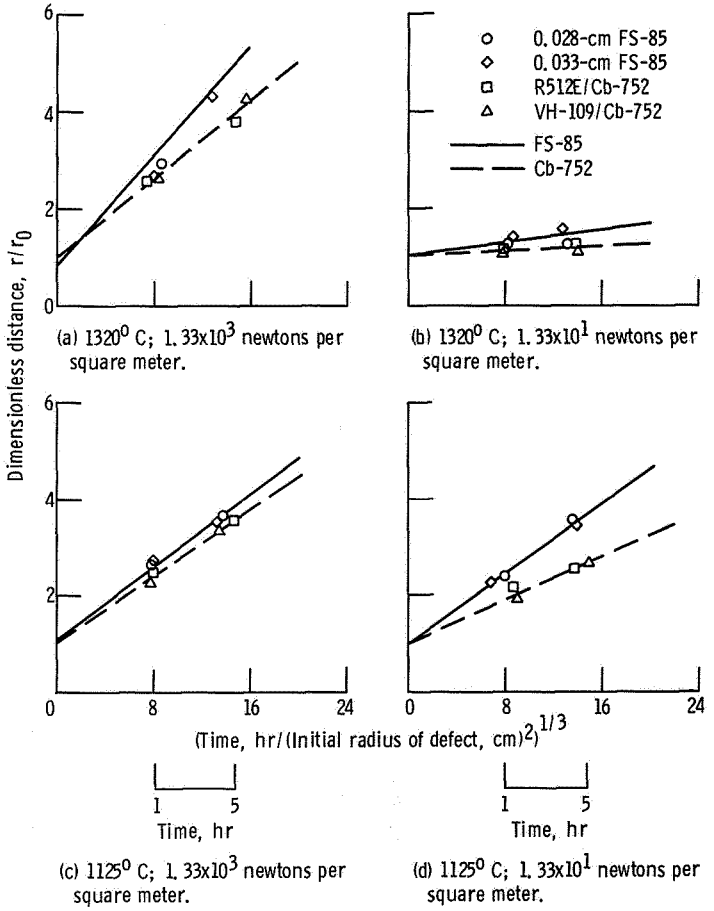

(a) 1320° C; 1.33x10³ newtons per square meter.

(b) 1320° C; 1.33x10¹ newtons per square meter.

(c) 1125° C; 1.33x10³ newtons per square meter.

(d) 1125° C; 1.33x10¹ newtons per square meter.

Figure 8. - Interstitial contamination to $KHN_{200\,g}$ = 300 at through-hole defects in fused slurry silicide coated FS-85 and Cb-752.

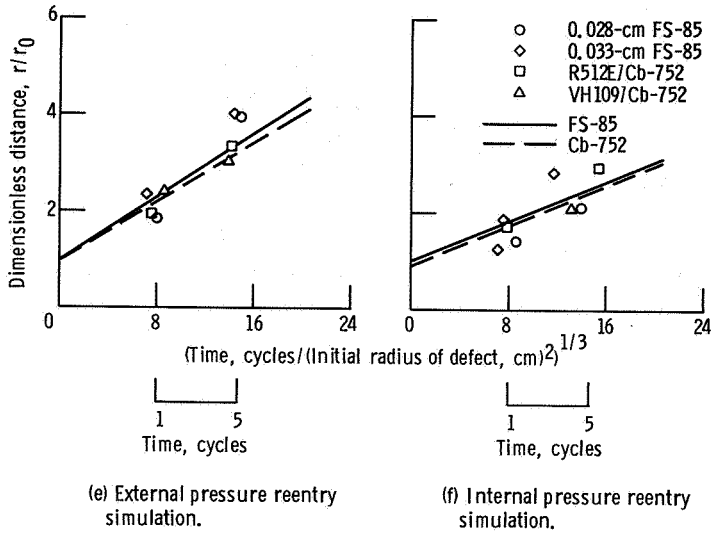

(e) External pressure reentry simulation.

(f) Internal pressure reentry simulation.

Figure 8. - Concluded.

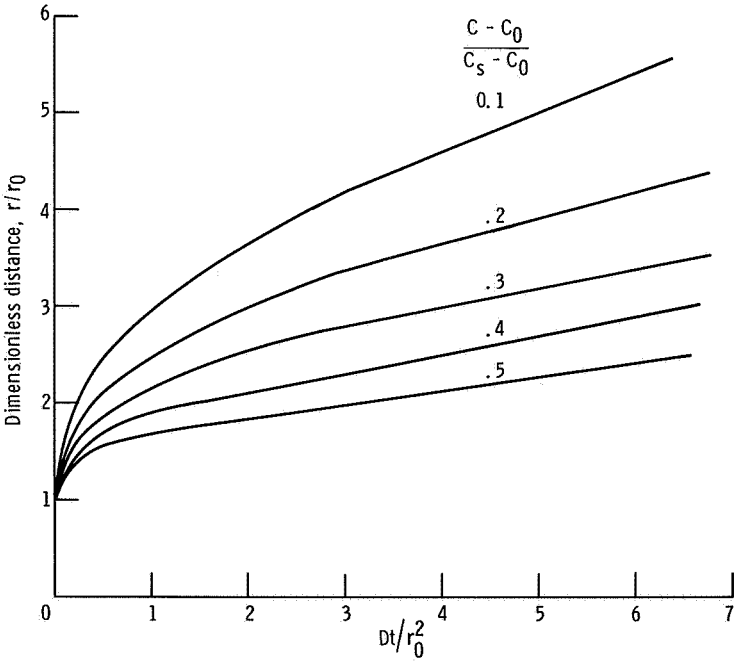

Figure 9. - Growth of cylindrical zone bounded internally by surface $r = r_0$ from reference 8.

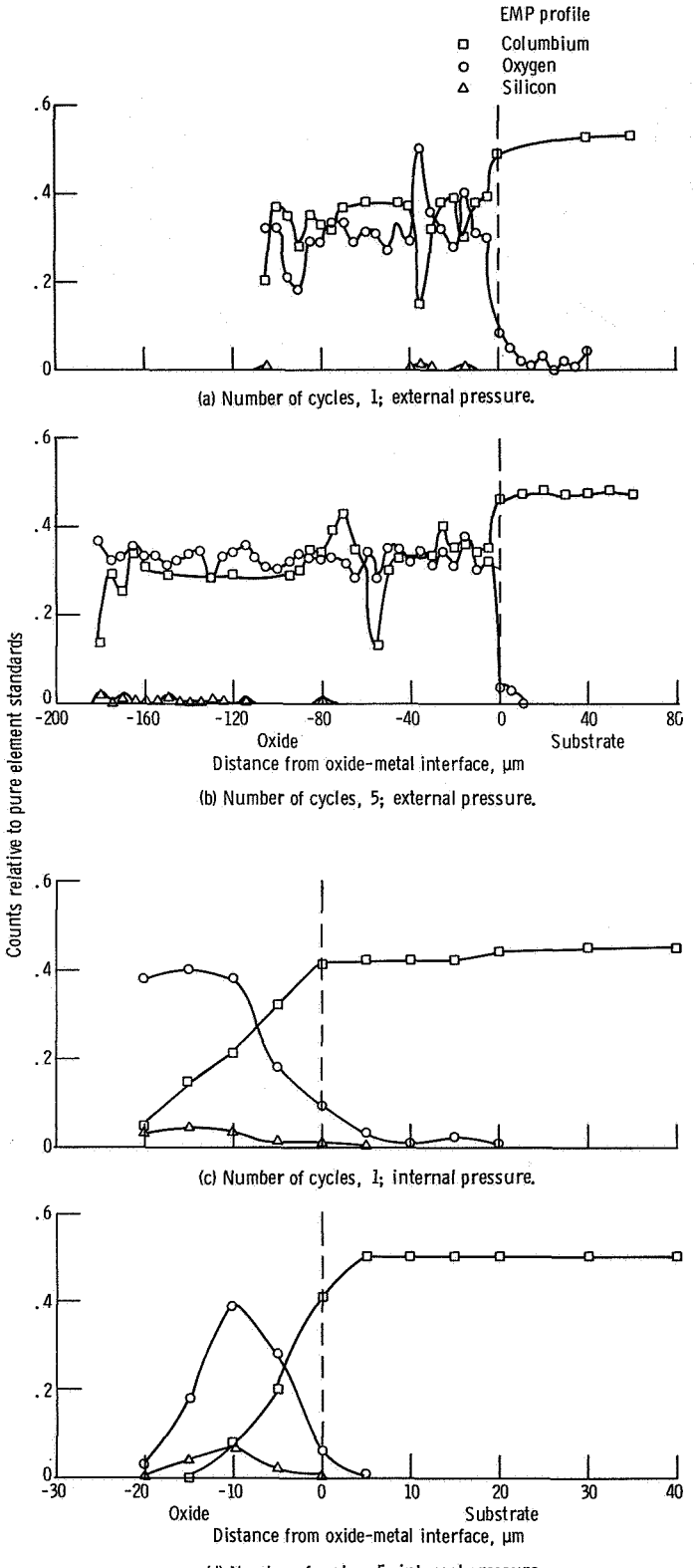

(a) Number of cycles, 1; external pressure.

(b) Number of cycles, 5; external pressure.

(c) Number of cycles, 1; internal pressure.

(d) Number of cycles, 5; internal pressure.

Figure 10. - EMP concentration profiles for defected R512E coated FS-85 after exposure to 1320° C simulated reentry exposures.

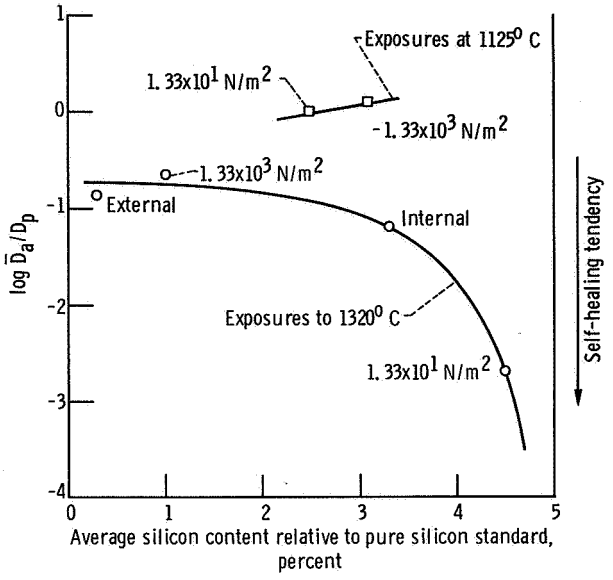

Figure 11. - Self-healing at 0.08-centimeter through-hole defects in FS-85 as function of silicon content of oxide grown at defect.

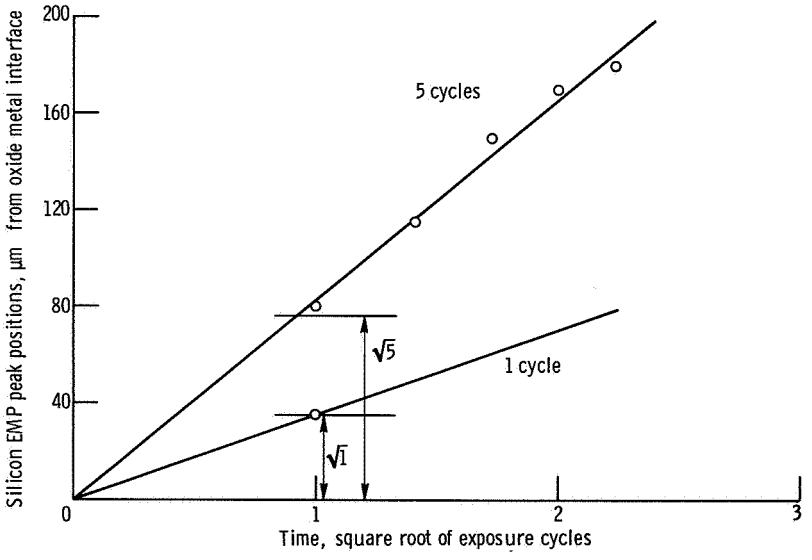

Figure 12. - Locations of silicon in oxides formed at defects in Si-20Cr-20Fe coated FS-85 exposed to external pressure reentry simulation cycles.

NATIONAL AERONAUTICS AND SPACE ADMINISTRATION
WASHINGTON, D.C. 20546

OFFICIAL BUSINESS
PENALTY FOR PRIVATE USE $300

SPECIAL FOURTH-CLASS RATE BOOK

POSTAGE AND FEES PAID
NATIONAL AERONAUTICS AND SPACE ADMINISTRATION
451

U.S.MAIL

POSTMASTER: If Undeliverable (Section 158 Postal Manual) Do Not Return

"The aeronautical and space activities of the United States shall be conducted so as to contribute . . . to the expansion of human knowledge of phenomena in the atmosphere and space. The Administration shall provide for the widest practicable and appropriate dissemination of information concerning its activities and the results thereof."

—NATIONAL AERONAUTICS AND SPACE ACT OF 1958

NASA SCIENTIFIC AND TECHNICAL PUBLICATIONS

TECHNICAL REPORTS: Scientific and technical information considered important, complete, and a lasting contribution to existing knowledge.

TECHNICAL NOTES: Information less broad in scope but nevertheless of importance as a contribution to existing knowledge.

TECHNICAL MEMORANDUMS: Information receiving limited distribution because of preliminary data, security classification, or other reasons. Also includes conference proceedings with either limited or unlimited distribution.

CONTRACTOR REPORTS: Scientific and technical information generated under a NASA contract or grant and considered an important contribution to existing knowledge.

TECHNICAL TRANSLATIONS: Information published in a foreign language considered to merit NASA distribution in English.

SPECIAL PUBLICATIONS: Information derived from or of value to NASA activities. Publications include final reports of major projects, monographs, data compilations, handbooks, sourcebooks, and special bibliographies.

TECHNOLOGY UTILIZATION PUBLICATIONS: Information on technology used by NASA that may be of particular interest in commercial and other non-aerospace applications. Publications include Tech Briefs, Technology Utilization Reports and Technology Surveys.

Details on the availability of these publications may be obtained from:

SCIENTIFIC AND TECHNICAL INFORMATION OFFICE

NATIONAL AERONAUTICS AND SPACE ADMINISTRATION

Washington, D.C. 20546